Human cortical networking by probabilistic and frequency-specific coupling

Authors,Yuxiang Yan [a], Tianyi Qian [a], Xin Xu [b], Hao Han [a], Zhipei Ling [b], Wenjin Zhou [c], Hesheng Liu [d], Bo Hong [a e]

https://doi.org/10.1016/j.neuroimage.2019.116363 *Open access*

Cortical network map based on co-activation probability matched clinical mapping.

Envelop coupling in alpha/beta carrier frequency supported the brain-wide connectivity.

Resting network over alpha/beta carrier frequency resembled that of various tasks.

Resting ECoG predicted the frequency range and spatial map of resting fMRI network.

Abstract

Large-scale cortical networking patterns have been established based on the correlation of slow fluctuations of resting fMRI signals. However, the electrophysiological mechanism of cortical networking remained to be elucidated. With large-scale human ECoG recording, we developed a novel approach for functional network parcellation on the basis of probabilistic co-activation of cortical sites in spatio-temporal microstates. The parcellated networks were verified by electrical cortical stimulation (ECS) and somatosensory evoked potentials recording, which showed significantly higher accuracy than the traditional long-term correlation method. This provides direct electrophysiological evidence supporting the dynamic nature of cortical networking. Further analysis revealed that the brain-wide connectivity is likely established on the coupling of ECoG power envelop over a common carrier frequency ranging from alpha to low-beta (8–32Hz). Surprisingly, the cortical networking pattern over this specific frequency was found to be consistent across various tasks, which resembles the resting networks. The high similarity between the above functional network parcellation and the fMRI resting network atlas in individuals also suggested the slow power-envelope

coupling of band-limited neural oscillations as the electrophysiological basis of spontaneous BOLD signals. Collectively, our findings on direct human recording revealed a probabilistic and frequency specific coupling mechanism for large-scale cortical networking shared by task and resting brain.

Keywords

Functional network
ECoG
Resting state
Dynamic connectivity
Carrier frequency

1. Introduction

Human cortex orchestrates hundreds of distinct regions to form functional networks that supports rich and flexible cognitive functions (Glasser et al., 2016). One of the key challenges of cognitive neuroscience is to understand the macroscale operating and organizing principles at the cortical network level. In the past decade, the cortical network patterns have been successfully depicted in resting-state functional MRI (Fan et al., 2016; Glasser et al., 2016; Gordon et al., 2017; Wang et al., 2015; Yeo et al., 2011). Recently, it has been further demonstrated that the architecture of these functional networks is constantly changing throughout development and aging over a long-term time course (Beason-Held et al., 2009; Fair et al., 2008; Supekar et al., 2009) and even on a second to minute time-scale (Chang and Glover, 2010; Handwerker et al., 2012; Jones et al., 2012; Sakoglu et al., 2010; Smith et al., 2012). The functional connectivity patterns of human cortex were parsed into microstates and the temporal evolution of these microstates were also characterized and related to psychiatric disorders and consciousness states (Allen et al., 2014; Calhoun et al., 2014; Damaraju et al., 2014; Demertzi et al., 2019; Liu and Duyn, 2013). However, the time-varying resting connectivity studies have long been hindered by the slow nature of hemodynamic signals, and still lack electrophysiological evidence (Logothetis, 2008; Sirotin and Das, 2009). This study sought to reveal the underlying electrophysiological mechanism of the dynamic connectivity of human cortex.

Non-invasive electrophysiological techniques have been employed to tackle this problem in a few studies (Hipp et al., 2012; Jann et al., 2009; Mantini et al., 2007). Scalp EEG and fMRI simultaneous recording showed the temporal resemblance between the EEG oscillatory activity and fMRI time courses during the resting state (Mantini et al., 2007). An MEG study revealed a frequency-specific spatial correlation structure in the human brain (Hipp et al., 2012). However, both EEG and MEG studies suffered from the volume conduction effect of the human skull, which may cause spurious correlation patterns (Hipp et al., 2012; Vinck et al., 2011). In addition, in these studies, the network connectivity was often assumed to be stationary and the spatial correlation was estimated using signals across the entire recording session. Whether the electrophysiological connectivity of the resting human brain shares the nonstationarity observed by the fMRI remains to be unanswered. More critically, through what kind of communication scheme the cortical regions are associated and form distinct functional networks has not yet been elucidated.

In this study, electrocorticography (ECoG) signals were directly recorded from the human cortical surface both in resting and various task states. With high temporal (millisecond) and spatial resolution (millimeter) and being less prone to the volume conduction of the skull, the time-varying functional connectivity patterns among cortical sites were estimated and then clustered into electrophysiological microstates (EMS). We hypothesized that cortical regions may interact in a probabilistic manner: the more often two regions jointly participate in the same microstates, the greater chance for them to form a functional network. Thus, the cortical regions were assembled as distinct networks on the basis of the probability of co-activation across these microstates. The parcellated cortical networks with this probabilistic approach matched well with functional maps derived from electrical cortical stimulation (ECS) and somatosensory evoked potentials (SSEP) with an accuracy of 83%, which was superior to the conventional approach based on a static correlation analysis. Furthermore, the co-activation of cortical regions in resting state was found to be driven by envelop coupling over the carrier frequency in alpha-beta range (8–32 Hz). The ECoG signal envelope in the coupling frequency band falls into the same frequency range of the BOLD fluctuation in the resting state, and the spatial pattern of the ECoG-based parcellation corresponds well with that of the resting-state fMRI network. Together, these results suggest a probabilistic and frequency-specific coupling mechanism for cortical

networking, which may not only explain the dynamic connectivity widely observed in resting-state fMRI (Allen et al., 2014), but also hint for new insights of whole-brain modeling and functional simulation (Wang et al., 2019).

2. Materials and methods

2.1. Subjects

Seventeen patients (9 males and 8 females, age 17.6 ± 4.9) with intractable epilepsy undergoing invasive monitoring for the localization of epileptogenic foci participated in the study (Table S1). Subdural electrode arrays (4-mm diameter, 10-mm interelectrode spacing) were temporally placed for the presurgical localization of seizure foci and mapping of cortical functions. This study was approved by the Ethics Review Committees at the School of Medicine, Tsinghua University, Tsinghua University Yuquan Hospital and the General Hospital of PLA. The placement of electrodes was fully based on clinical diagnoses. Consent was given by all of the patients before the experiments, following the procedures of the hospitals and Ethics Review Committees mentioned above. Experiments were conducted during stable interictal periods. Patients with apparent anatomical lesions or having epileptic seizures within 1 h before or after the experiments were excluded.

2.2. ECoG experiments

The resting, as well as a series of task experiments was conducted to obtain the intrinsic and task-evoked ECoG responses. Resting state signals were recorded while the participants passively fixated on a visual crosshair centered on the screen for 5 min (S1, S4, S5, S7–S9, S12–S17) or 10 min (S2, S3, S6, S10, S11). The task experiments consist of 7 conditions including motor mapping, picture naming, silent reading, picture encoding, picture recall, word encoding and word recall. The motor-mapping task was designed as a block-design experiment (Qian et al., 2013). In each block, the participants were instructed to make a hand or tongue movement. The hand and tongue task blocks were both repeated 10 times. For the picture naming task, participants were instructed to name the pictures loudly following the pictures being shown on the screen (Flinker et al., 2015). In the silent reading task, participants were instructed to read several

paragraphs silently (Flinker et al., 2015). The memory task included two sessions: the first session was encoding, with participants looking at pictures or words on the screen and judging whether they are living or non-living; after 30 min, in the recall session, the participants were instructed to judge whether the pictures or words on the screen were shown before in the encoding phase (Vilberg and Rugg, 2008; Zhang et al., 2018).

2.3. ECoG data acquisition

ECoG signal recordings were performed by two types of long-term video EEG monitoring systems: A Bio-Logic 128-channel ECoG monitoring system at the Epilepsy Center of Tsinghua Yuquan Hospital and a Necolet C64 ECoG monitoring system at the Department of Functional Neurosurgery of Chinese PLA General Hospital with a sampling rate of 1024 Hz. The stimulus presentation and response collection of all tasks were controlled by MATLAB Psychtoolbox (Kleiner et al., 2007). Four inactive epidural electrodes placed on the inner surface of the skull were employed as ground and reference (two for ground and two for reference) (Si et al., 2017).

2.4. Electrode localization

ECoG electrodes were localized on the individual cortical surface by combining a pre-operative T1-MRI and post-operative CT images (Si et al., 2017). For each patient, the structural MRI was acquired before ECoG electrode implantation using a three-dimensional T1 sequence (TR = 2000 msec, TE = 2.37 msec, flip angle = 90°, slice number = 180, 1-mm isotropic voxels). The pial surface was reconstructed using T1-weighted images in Freesurfer (Fischl et al., 2002). A post-implantation CT scan was acquired to identify the locations of the electrodes and the skull. The locations of the electrodes in CT images were labeled manually. As described in our previous study (Si et al., 2017), the coordinates of the ECoG electrodes were automatically projected to the pial surface by co-registering the CT and MRI images using a mutual information-based algorithm in Freesurfer (Qian et al., 2013). For Subject S8 and S9, only CT images were acquired, and the electrode locations of these two subjects were mapped on the MRI cortical template with CT images (Miller et al., 2007).

2.5. ECoG signal processing

All the data analyses of acquired ECoG signal were performed in MATLAB (MathWorks). First, the power line noise (50 Hz) as well as its harmonics were first notch-filtered in the recorded data, and the channels within ictogenic zone identified in the clinic were excluded. For the resting state analysis, to investigate the frequency specificity of large-scale cortical connectivity, the notch-filtered raw signal was bandpass filtered into a narrow-band signal using a two-way zero phase lag Butterworth filter, with the central frequencies spaced logarithmically according to the exponentiation of base 2 with exponents ranging from 1 to 6 in steps of 1/4 (Hipp et al., 2012). The analytic amplitude of each narrow band time series was extracted using the Hilbert transform and then squared to obtain the power envelope (Cheung et al., 2016). The power envelope signal was then downsampled to 64 Hz. The power envelope was further resolved using Morlet's wavelet in the analysis of the connectivity value as a function of the carrier as well as power-envelope frequencies (Hipp et al., 2012). For the task state analysis, the notch-filtered raw time series was bandpassed into a series of broadband signals, including delta (2–4 Hz), theta (4–8 Hz), alpha (8–16 Hz), beta (16–32 Hz), gamma (32–64 Hz) and high gamma (60–140 Hz) bands by zero-phase lag FIR filters (Foster et al., 2015).

2.6. ECoG parcellation

Based on our hypothesis that the functional connectivity strength among the cortical regions could be measured by the probability of these regions "co-activating" in multiple microstates, we proposed a co-activation probability (CAP) approach to estimate the cross-regional functional connectivity. The CAP approach included two stages as follows: (1) Temporal clustering of microstates. To capture the time-varying functional correlation between two cortical regions, the resting ECoG signals were first band-pass filtered in alpha-beta band (8–32Hz). To find the best frequency band, we also performed band-pass filtering for each frequency band in the range of 2–64Hz, as described in Section 2.5. Then the power envelope was cut into short-time segments (with a 5-s width and 1.25-s step, Fig. 1A). In each segment, the Pearson's correlation of the bandpassed power envelope was computed between each electrode pair (Fig. 1B). All columns in the lower triangle of each segment's paired correlation matrix were

concatenated as a correlation vector. All the segments were then temporally clustered into ten microstates by k-means clustering algorithm on the basis of the squared Euclidean distance of their correlation vectors (Fig. 1C and D)(MacQueen, 1967). The number of clusters was determined by two criteria: (i) the ratio of between-cluster scatter (Sb) and the within-cluster scatter (Sw) and (ii) the stability of micro-state occupancy (Fig. S1). The Sb and Sw were defined as:where is the number of clusters, N is the number of all vectors, N_i is the number of vectors in each cluster i, and represents the short-time correlation vector j in cluster i, , (Härdle and Simar 2007). The stability of clustered micro-states was calculated by cutting the resting state into two equal-length durations and comparing the consistency of occupancy of microstates (Calhoun et al., 2014). The electrodes in each microstate were spatially parcellated into 5 subnetworks by k-means clustering based on their averaged correlational patterns, which included approximately 20% of the prominent correlations from the overall correlation pairs, and these clustered electrodes were regarded as the co-activated functional regions in this microstate (Fig. 1E). (2) Spatial parcellation based on CAP. All the microstates were then assembled into the functional connectivity matrix: each CAP value in the matrix was represented by the probability of the corresponding electrode pair being co-activated during the resting state:where is the number of micro-states, is the number of segments of micro-state , and denotes whether electrode a and b are clustered into the same subnetwork () or not () using the mean connectivity matrix of micro-state . Finally, the functional connectivity matrix based on the paired co-activation probability was clustered into 5–8 networks. The parcellation patterns with 7 networks were represented.

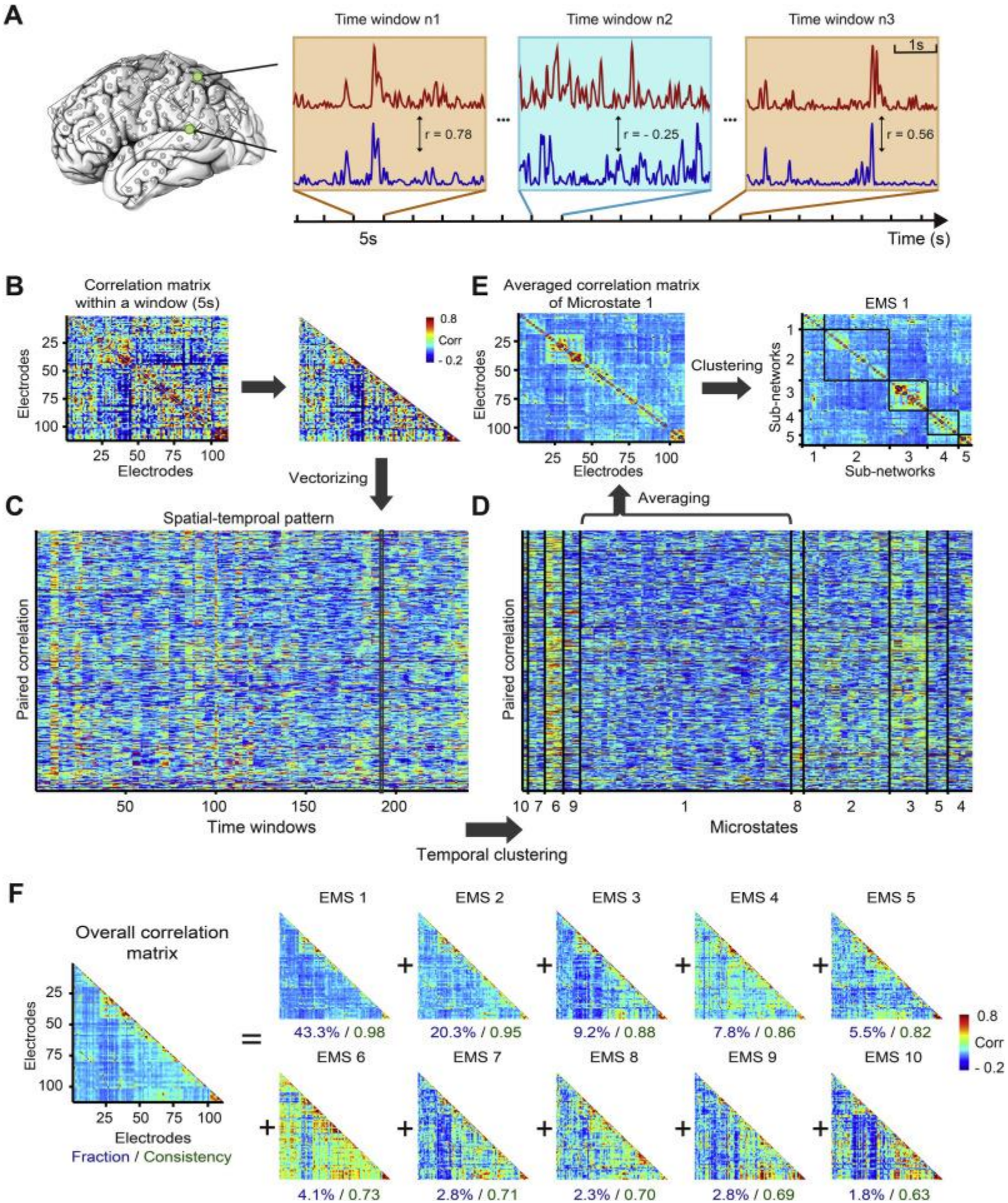
A
Time window n1
Time window n2
Time window n3
1s
r = 0.78
r = - 0.25
r = 0.56
5s
Time (s)
B
Correlation matrix within a window (5s)
Electrodes
0.8
Corr
- 0.2
Vectorizing
C
Spatial-temproal pattern
Paired correlation
Time windows
D
Averaging
Paired correlation
Microstates
Temporal clustering
E
Averaged correlation matrix of Microstate 1
Clustering
EMS 1
Sub-networks
F
Overall correlation matrix
Fraction / Consistency
EMS 1
EMS 2
EMS 3
EMS 4
EMS 5
43.3% / 0.98
20.3% / 0.95
9.2% / 0.88
7.8% / 0.86
5.5% / 0.82
EMS 6
EMS 7
EMS 8
EMS 9
EMS 10
4.1% / 0.73
2.8% / 0.71
2.3% / 0.70
2.8% / 0.69
1.8% / 0.63

Fig. 1. Temporal clustering of time-varying connectivity patterns into microstates. (A). The power envelope extracted from the ECoG electrodes of an exemplary patient was in varying correlational structures across time windows. (B). The paired-correlation matrix of frequency band limited ECoG signals in a short-time segment (5s). (C). The lower triangular matrix of each correlation matrix is reshaped into a vector. All the vectors are assembled into the spatial-temporal pattern representing the time-varying connectivity of brain wide electrodes. (D). The spatial-temporal pattern is temporally clustered into ten electrophysiological microstates (EMS) in accordance to the vectorized correlation matrix of the short-time segments. (E). The correlations of each ECoG electrode pair within a microstate are averaged to constitute the mean correlation matrix, which is then spatially clustered into five sub-networks. (F). The mean paired correlational patterns of the ten EMSs, ranked by their consistency values with the overall paired correlational pattern. Both consistency and fraction values are shown below each EMS.
To examine whether the CAP approach could better reflect the cross-regional functional connectivity in the time-varying rest state, the cortical surfaces covered by the electrodes were also parcellated into functional networks by using the conventional power envelope correlation (PEC) analysis method, as has been done with in previous fMRI, MEG/EEG studies (Biswal et al., 1995; Calhoun et al., 2014; Hipp et al., 2012; Mantini et al., 2007; Vincent et al., 2007; Yeo et al., 2011). In the PEC method, the Pearson's correlation coefficient of the power envelope of the entire bandpassed time series was used to represent the functional connectivity value of electrode pairs.

2.7. Statistical measures for validity test

We applied two clinical functional mapping techniques, the electrical cortical stimulation (ECS, in Subject 1–5, 7 and 9) and somatosensory evoked potentials (SSEP, in Subject 6 and 8) as references for validating the above CAP parcellation algorithm (Table S2). The sensitivity, specificity and accuracy (F1 score) were adopted as the performance measurements, defined as the equations below (Fawcett, 2006):where TP, FN, TN, FP represent the true positive, false negative, true negative and false positive results, respectively.
A permutation test was conducted to exclude the possibility that the consistency of the parcellated and ECS localized networks was caused by random factors. In the

permutation test, we presented the ECS/SSEP localized regions at random positions but with consistent electrode numbers, region shapes and spacing, and then evaluated their consistency with the ECoG-based parcellated functional network patterns. All the other aspects in the permutation test for network parcellation and ECS/SSEP comparison were kept the same. The above consistency measurements in the random-position ECS/SSEP were used as the chance level in the permutation test.

2.8. fMRI data acquisition and preprocessing

A 12-min resting fMRI signal (with two 6-min sessions) was recorded in four subjects (S2, S3, S5 and S7), with the same paradigm as in the resting ECoG experiment. All fMRI experiments were carried out on a Philips Achieva 3.0T TX scanner. Functional MR images were acquired using echo planar imaging sequences (TR = 3000 msec, TE = 30 msec, slice number = 47, 3-mm isotropic voxels). The functional MR images were preprocessed with a series of steps following previous studies (Wang et al., 2015; Yeo et al., 2011), including: 1) discarding the first four volumes of each run to allow for T1-equilibration effects, 2) compensating for slice acquisition-dependent time shifts per volume with SPM2 (Wellcome Department of Cognitive Neurology, London, UK), 3) correcting for head motion using rigid body translation and rotation with the FSL package (Jenkinson et al., 2002; Smith et al., 2004), 4) resampling the data with a 2-mm cubic voxel, 5) temporal filtering to remove constant offsets and linear trends over each run but retaining frequencies below 0.08 Hz, 6) spatial smoothing using a 4-mm full-width half-maximum Gaussian blur, 7) and regressing out several sources of spurious or regionally nonspecific variances (six-parameter rigid body head motion obtained from motion correction, the signal averaged over the whole brain, the signal averaged over the lateral ventricles, and the signal averaged over a region centered in the deep cerebral white matter).

2.9. Comparison of ECoG and fMRI network parcellation

A subject-specific functional network parcellation algorithm developed in our previous study was used to parcellate the cortical regions of each subject into 18 functional networks (Wang et al., 2015; Wang and Liu, 2014). In comparison to the ECoG parcellation, the fMRI functional networks were masked to match the ECoG coverage

and discretized into dots with the same anatomical locations as the ECoG electrodes. The Dice coefficient was applied to evaluate the spatial pattern similarity between the resting ECoG and fMRI-based parcellations (Wang et al., 2015; Wang and Liu, 2014).

2.10. ECS/SSEP experiments

The clinical electrical cortical stimulation (ECS) experiment was performed to identify the cortical regions causing seizure sensations or engaging in crucial (such as motor or language) brain functions. The electrical stimulation was generated by an Ojemann Cortical Stimulator (Integra Life-Sciences), and delivered to 2 adjacent ECoG electrodes by bipolar square waveform (pulse width: 0.3 ms, frequency: 60 Hz, duration: 2–5 s, current intensity: 2–15 mA, Qian et al., 2013; Zhang et al., 2019). The seizure- and function-related responses of the participants were recorded by physicians during the ECS experiments. The clinical somatosensory evoked potential (SSEP) test was performed to map the somatosensory functional network, by delivering a series of current pulse to the median nerve at the wrist with the 200 ms pulse width and 15 mA current intensity.

2.11. Data and code availability

The data and codes that support the findings of this study are available upon request.

3. Results

3.1. Functional networking via probabilistic co-activation

Seventeen epilepsy patients with ECoG implantation were included in this study (Table S1). To capture the time-varying functional correlation between two cortical regions, the power envelopes of frequency band-limited resting ECoG signals were cut into short-time segments (5 s) using sliding windows. Taking alpha-beta band (8–32Hz) as an example, the nonstationary correlation was found between the fluctuations of the power envelopes among electrode sites during the resting state (Fig. 1A). It is noticeable that, for some period of time, the power envelope of the two electrodes exhibited a strong correlation (shown in light brown), while for other time windows, the correlation

was weak (shown in light cyan). Based on this observation, all the short-time segments were then clustered into ten groups, according to the similarity of the correlation patterns between electrode pairs in each segment (Fig. 1B–E). Since each group had a distinct functional correlation pattern and a certain probability of occurrence in time, we named them “electrophysiological microstates” (EMS). In the example shown in Fig. 1F, EMS 1 and EMS 2 occupied the major part of the time (43.3% and 20.3%, respectively).

Based on the hypothesis that the functional connectivity strength among the cortical regions could be represented by the probability of these regions co-activating in multiple microstates, we built a co-activation probability (CAP) matrix to reflect the relations among electrodes during the nonstationary resting state (Fig. 2A). Using the CAP matrix, the cortex covered by electrode grids was then parcellated into functional networks. Notably, parcellated networks in the exemplary cortex closely resembled well-defined functional networks such as the visual, motor, language and attention networks (Fig. 2B).

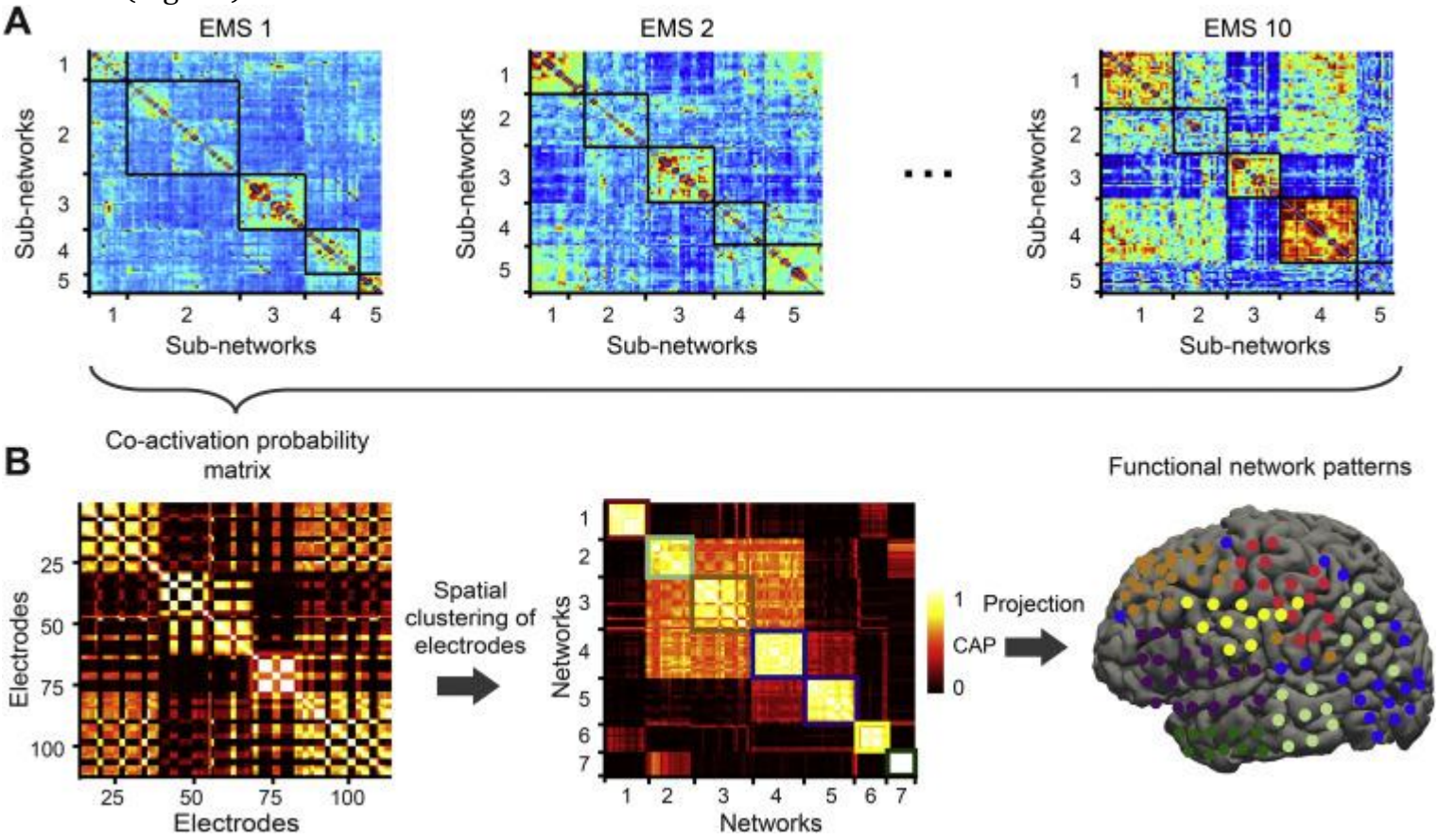

Fig. 2. Spatial clustering of electrodes into functional networks. (A). The microstates were assembled to form the co-activation probability (CAP) matrix according to the probability of each electrode pair falling in the same sub-networks across microstates. (B). The CAP matrix (left panel) was then parcellated into 7 functional networks. Electrode pairs in each frame corresponded to a functional network (medial panel) and was projected on the cortical surface (right panel). The positions of electrodes were registered by combining CT and structural MRI images.

To validate the above CAP approach, the resulted network patterns were compared with the cortical networks localized by electrical cortical stimulation (ECS) and somatosensory evoked potentials (SSEP). Fig. 3A illustrated the cortical parcellation patterns based on the individualized frequency band for each participate that match ECS/SSEP localization best. Taking S5 as an example, the tongue and hand-related electrodes were mapped by ECS. Our CAP approach revealed high intranetwork co-activation probability values (in yellow) and low internetwork values (in dark blue), with gaps resembling the boundaries localized using ECS (Fig. 3B). The within-network correlation values were also higher than the between-network correlation values (Fig. 3B). The sensitivity, specificity and accuracy were 0.930.10, 0.960.03 and 0.830.06 (meanS.D., Fig. 3C, Table S2), respectively, which were significantly higher than the permutation test results ($P < 10^{-6}$, 0.05, and 10^{-6}, respectively).

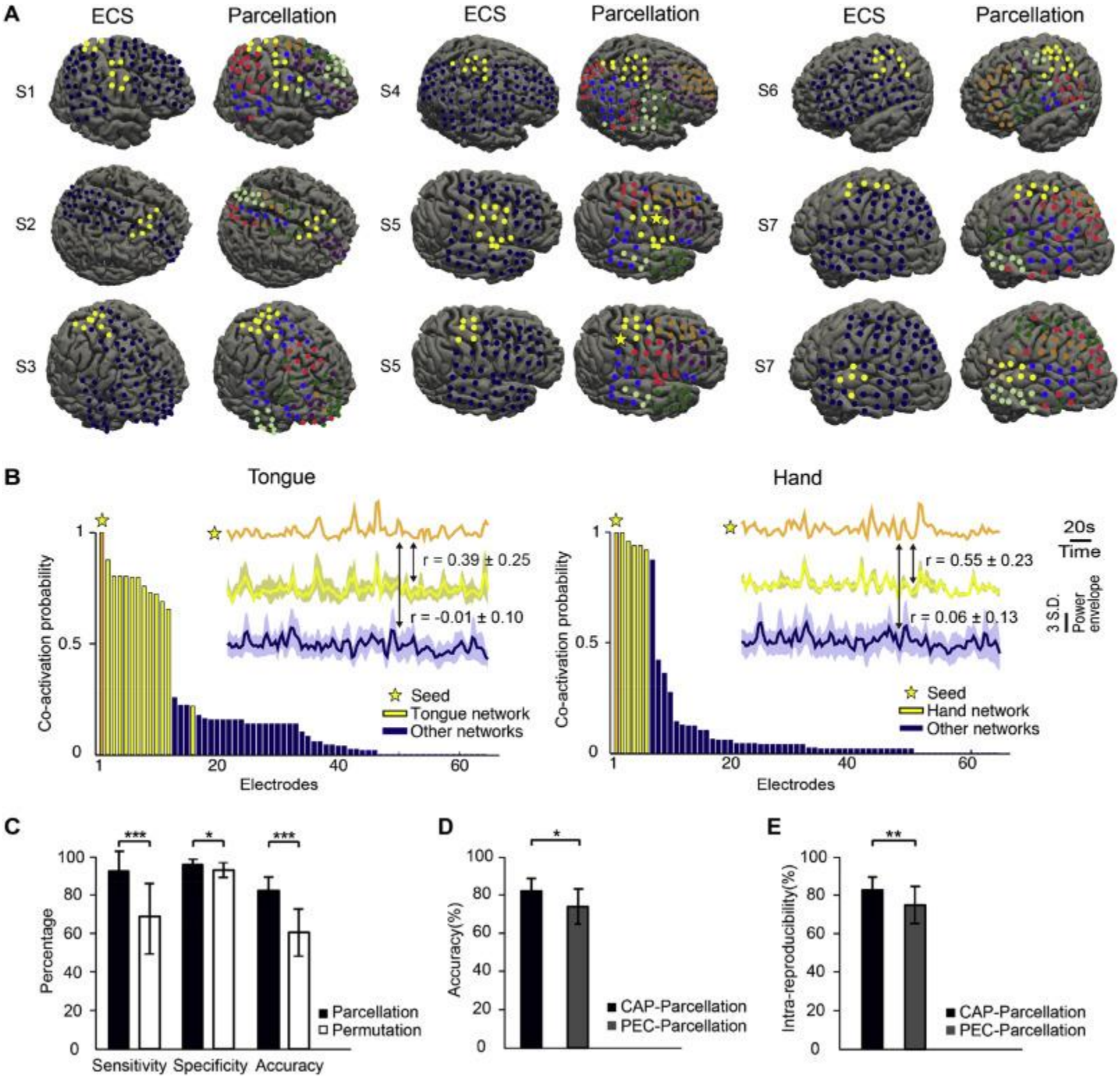
A
ECS
Parcellation
ECS
Parcellation
ECS
Parcellation
S1
S4
S6
S2
S5
S7
S3
S5
S7
B
Tongue
Hand
Co-activation probability
Electrodes
r = 0.39 ± 0.25
r = -0.01 ± 0.10
r = 0.55 ± 0.23
r = 0.06 ± 0.13
Seed
Tongue network
Other networks
Hand network
20s
Time
3 S.D.
Power envelope
C
Percentage
Sensitivity
Specificity
Accuracy
Parcellation
Permutation
D
Accuracy(%)
CAP-Parcellation
PEC-Parcellation
E
Intra-reproducibility(%)
CAP-Parcellation
PEC-Parcellation

Fig. 3. Validation of the CAP-based functional network parcellation. (A). The cortical network parcellation with CAP approach using resting ECoG, and the areas localized by electrical cortical simulation (ECS) and the somatosensory evoked potential (SSEP). The blue dots in the ECS/SSEP mappings (left column) indicate the negative electrodes, and the yellow dots indicate the positive electrodes. In the parcellation mappings (right column), electrodes with the same color are in the same functional networks, and the yellow shows networks corresponding to the ECS/SSEP results. (B). The co-activation probability (CAP) values seeded by two exemplary electrodes in the hand and tongue regions identified by ECS of S5 (indicated by yellow star). The electrodes inside and outside the two functional networks are shown in yellow and dark blue, respectively. The intra-network electrodes displayed strong CAP values as well as similar fluctuations of the power envelope. (C). The sensitivity, specificity and accuracy of the functional network parcellation. ECS and SSEP were used to evaluate the accuracy of the resting ECoG functional parcellation in all nine patients having ECS/SSEP localization. The performance of CAP parcellation were significantly higher than that of the permutation test (*$P < 0.05$, ***$P < 10^{-6}$, one-tailed *t*-test). (D). The accuracy comparison of functional network parcellation using CAP and PEC approaches. The parcellation accuracy of CAP approach was significantly higher than that of PEC (*$P < 0.01$, one-tailed *t*-test), and both methods show significantly higher accuracy than permutation test (**$P < 10^{-4}$ and ***$P < 10^{-6}$, respectively, one-tailed *t*-test). (E). The intrasubject reliability of the CAP and PEC approaches was measured by comparing the parcellation results using two independent resting sessions in the same patients. The CAP approach possessed a significantly higher reliability than the PEC (*$P < 0.001$, one-tailed *t*-test). All error bars denote SD.

We further tested whether our CAP approach with the consideration of probabilistic connections could better reflect the functional network patterns than the correlation of spontaneous fluctuations estimated over the entire time, as has been done with the power envelope correlation (PEC) analysis in previous fMRI, MEG/EEG studies (Calhoun et al., 2014; Hipp et al., 2012; Mantini et al., 2007). Functional networks were separately parcellated by both the CAP- and PEC-based approaches in the individuals, and the parcellation accuracy was compared. We found a significantly higher accuracy for the parcellation by the CAP approach than for that by the PEC approach (0.740.09, meanS.D., $P < 0.01$, Fig. 3D). The intrasubject test-retest reliability values were

compared as well. We recorded two independent sessions (with the same data-length) at rest in seven patients, and the test-retest reliability was evaluated as the Dice coefficient of the networks obtained from the two sessions. We found that the reliability of the CAP approach (r = 0.810.07, meanS.D.) was significantly higher than that of the PEC approach (r = 0.740.10, meanS.D., P < 0.001, Fig. 3E). The higher accuracy and reliability of co-activation probability approach in parcellating cortical networks favored our probabilistic coupling model over the stationary one in cortical networking.

3.2. Frequency specificity of dynamic connectivity in resting state

We further investigated whether there exist specific frequencies in ECoG signals that are dominant in the probabilistic envelop coupling observed at rest. The normalized power spectral densities (PSDs) of electrodes in functional networks mapped by ECS (including electrodes in the frontal eye field, hearing and sensorimotor areas) exhibited clear peaks in the range of the alpha to beta bands (8–32 Hz) during the resting state (Fig. 4A). To test whether different functional networks use specific carrier frequencies for their intra-network communication, we evaluated the parcellation performance in all subjects by band-passing the ECoG signal with different carrier frequencies ranging from the delta to gamma bands (2–64 Hz). We found that the functional parcellation over the carrier frequency of alpha to beta bands (8–32 Hz) closely matched the ECS/SSEP localized maps, especially for the sensorimotor regions, while the carrier frequencies for the hearing network and frontal eye field were significantly lower than those for the sensorimotor regions (Fig. 4B, P < 0.05 and P < 0.001, respectively). Using the frequency range of alpha to beta as the carrier, we could obtain a reasonably good accuracy for the functional network parcellations (Fig. 4C, Dice coefficient = 0.740.09, meanS.D., $p < 10^{-6}$, permutation test).

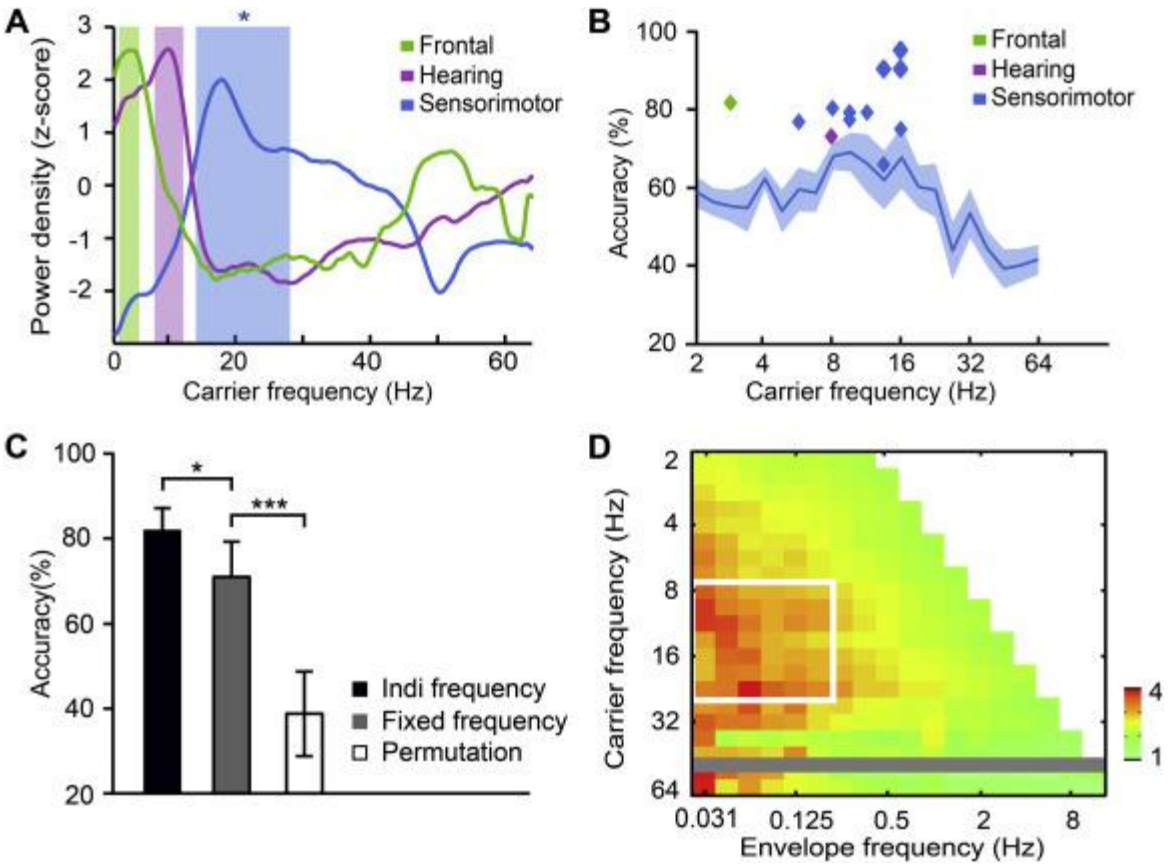

Fig. 4. Frequency-divided communication in resting networks. (A). The power density of distinct functional networks (green for frontal eye field, purple for hearing region, and blue for sensorimotor region), with the baseline of the mean power density outside the corresponding functional regions. The power density function of sensorimotor region displays peak around the alpha to beta frequency range (Shaded bar, FDR correction, *q < 0.05). (B). The parcellation results in the nine patients with ECS/SSEP verifications were projected on the plane of carrier frequency and accuracy. The position of each dot corresponds to the individualized carrier frequency and the parcellation accuracy for each subject. The averaged parcellation accuracy of the sensorimotor networks with a standard error mean was shown as the blue curve. (C). The comparison between parcellation accuracy with fixed carrier frequency (8–32 Hz) and with the individualized carrier frequency (*P < 0.01, ***P < 10^{-6}, paired *t*-test). All error bars denote SD. (D). Connectivity value in functional networks as a function of the carrier frequency and the envelope frequency. Intranetwork connectivity value is averaged in all subjects and normalized by the mean connectivity value in the corresponding carrier

frequency. The range of carrier and envelope frequency that showed significant higher intra-network connectivity in comparison to the average level ($p < 0.05$, two-sample *t*-test) is enclosed by white box. The highest envelope frequency is bounded by the carrier frequency, and the carrier frequency of power line (50 Hz) was eliminated (in dark gray).

The above observation of the carrier frequency specificity suggested a scheme of frequency-divided communication for the cortical functional networks. On top of the carrier frequency, we also checked the property of power-envelope signals. The CAP-based functional connectivity was then resolved as a function of the carrier frequency and power-envelope frequency (Hipp et al., 2012). We obtained the connectivity strength in the same parcellated networks in each specific carrier and power-envelope frequency and averaged the result across all 17 subjects. In each frequency bin, the connectivity value was normalized by dividing the mean short-time correlation of the power envelope at corresponding carrier frequency. The carrier frequencies having the strongest connectivity value were found to be in the range of 8–32 Hz, which is consistent with the best carrier frequency range for the individual cortical parcellation (Fig. 4D). Surprisingly, the highest ECoG power envelope resided in the frequency range lower than 0.125 Hz, which matched well with the main frequency range of the resting hemodynamic signal in fMRI (<0.1 Hz)(Cordes et al., 2001; Fox et al., 2016).

We further compared the spatial patterns of the resting functional networks obtained using ECoG and fMRI signals (Ojemann et al., 2013). Four of the subjects participated in resting fMRI scan, and 18 functional networks were mapped onto the whole cortex using a subject-specific network parcellation approach (Wang et al., 2015). There exists a significant spatial overlap between the ECoG-based and fMRI-based network parcellations (Fig. 5, Dice coefficient = 0.590.07, meanS.D.). We also performed the CAP cortical parcellation using the high-gamma band (60–140Hz) of resting ECoG signals, and compared the results with the cortical atlases acquired by fMRI. We found that the high-gamma band-based ECoG cortical parcellation results showed less similarity to corresponding fMRI-based cortical atlases (Dice coefficient = 0.41 ± 0.09, mean ± S.D.), which was significantly lower than that of alpha-beta band parcellations ($P < 0.01$, paired *t*-test).

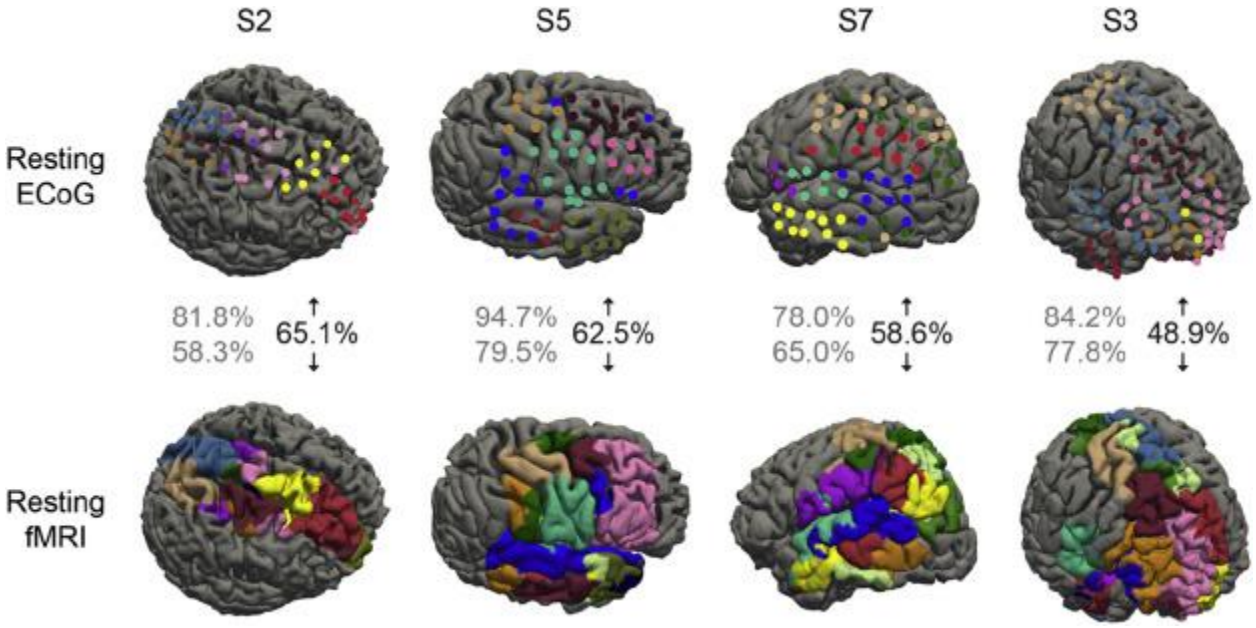

Fig. 5. Individual functional network parcellation using resting ECoG and resting fMRI. The cortical networks parcellated by ECoG CAP algorithm and resting fMRI. The percentage in light gray indicates the parcellation accuracy respectively, and the percentage in dark gray is the spatial pattern overlap between these two modalities.

3.3. Concordance of resting and task parcellation

fMRI studies have suggested that resting networks might lay the foundation for task responses (Cole et al. 2014, 2016; Tavor et al., 2016), and the resting networks may also be observed in task states, as we found in a previous study (Fox et al., 2016). However, the electrophysiological evidence of this rest-task crosstalk is scarce (Kucyi et al., 2018). With our ECoG data from various task states, task-evoked signals were bandpass filtered into the alpha-beta range (8–32 Hz) instead of the high-gamma band. Surprisingly, the functional networks carried on the alpha-beta band in all tasks resembled the resting network obtained with resting data on both left and right hemispheres (Fig. 6A). The functional networks of the task-free state and seven tasks were highly overlapped, with an average Dice coefficient of 0.75 (Fig. 6B).

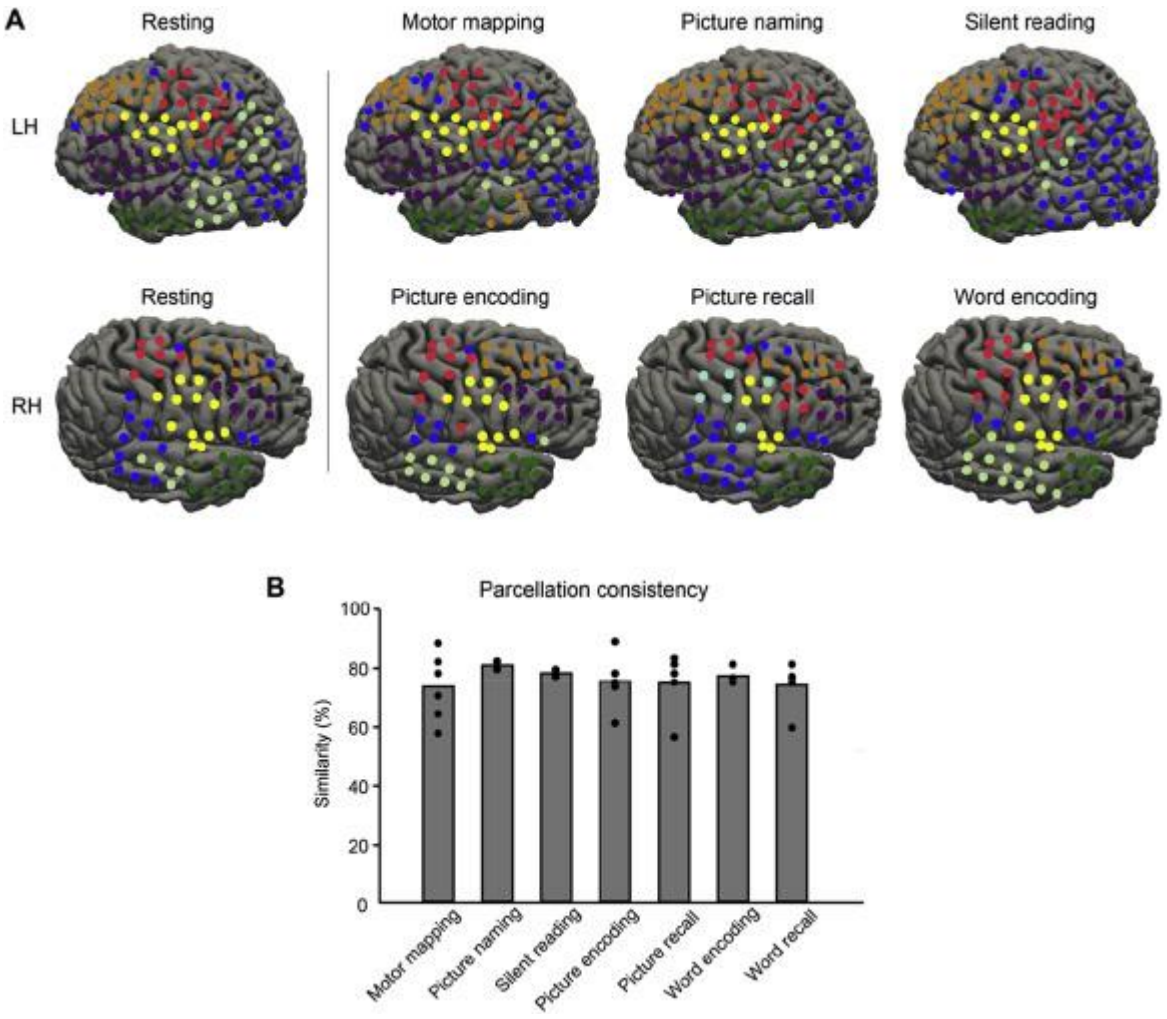

Fig. 6. Consistency of multitasks functional network parcellations. (A). The parcellation maps in the resting state and different tasks of two exemplary subjects (S12 and S5), with ECoG electrodes covering the left and right hemispheres, respectively. (B). Spatial pattern consistency of parcellation maps between the resting and various task states (30 task experiments with 7 task types in 9 patients) in the alpha to beta carrier frequency range. Each dot indicates a consistency value to the resting state of a single task, and each bar indicates the mean value of a specific task type across subjects.

It has been shown that the high-gamma activities above 60 Hz are tightly correlated with multi-unit neuronal firing, reflecting the local neural processing (Fries, 2009; Lachaux et al., 2012; Pei et al., 2011; Sinai et al., 2005; Womelsdorf et al., 2007). Here, we analyzed the ECoG responses during various task states (including motor mapping, picture naming, silent reading, picture encoding, picture recall, word encoding

and word recall) and found strong activation in the high-gamma range in the event-related spectrogram (Fig. 7A) and power spectral density (Fig. 7B), which is consistent with our previous ECoG findings (Qian et al., 2013; Si et al., 2017). We parcellated the functional networks by the CAP approach using the ECoG power envelope in the high-gamma band (60–140 Hz). Different functional connectivity patterns were observed between the resting and task states. For visualization, we projected the short-time connectivity matrix in different states to a two-dimensional space using principal component analysis (PCA). Taking high-gamma as the carrier frequency band, there exists an apparent separation between the resting and task states (Fig. 7C, notable separation along the axis of PC1). The distinctions among tasks are also evident, especially between motor and other cognitive tasks (along the axis of PC2). In contrast, the functional connectivity patterns over the carrier frequency of the alpha to beta range (8–32Hz) were insensitive to various tasks in the principal component space (Fig. 7D). This suggested a dual-band frequency multiplexing of the resting and task states for cortical connectivity, while the probabilistic co-activation scheme was shared by both.

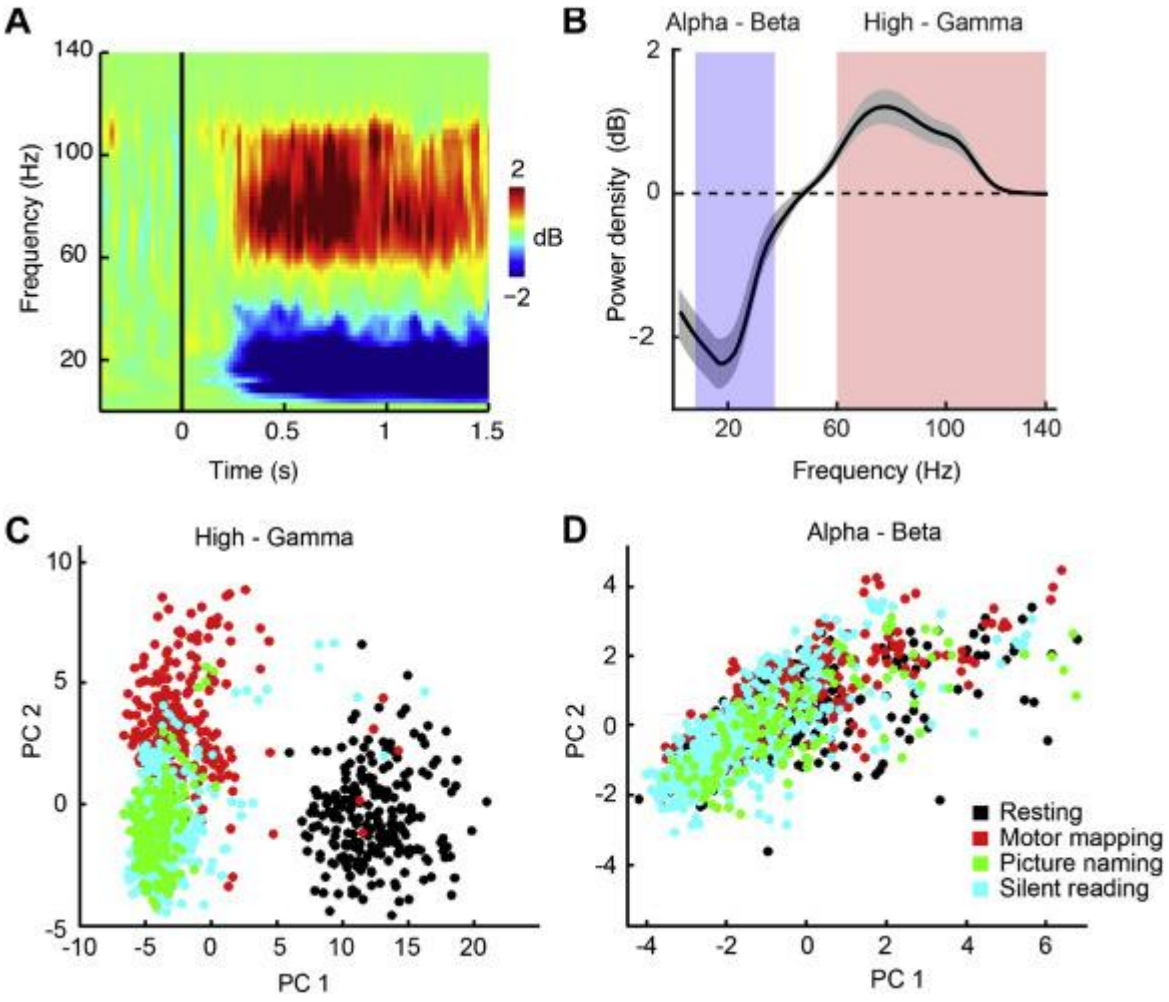

Fig. 7. Carrier frequency division between resting and task states. The event-related spectrograms (A). and power spectral density (B). of electrodes in the hand network during the motor task (hand grasping). Pink bar indicates the high-gamma (60–140 Hz) band, and blue bar indicates alpha to beta (8–32 Hz) bands. (C). Network connectivity patterns in the high-gamma band after projection to two-dimensional space using PCA. (D). Network connectivity patterns in alpha to beta range after projection to two-dimensional space using PCA.

4. Discussion

In this study, we proposed a dynamic mechanism of large-scale cortical networking, in which the connection between cortical regions are on the basis of the probabilistic coupling of spontaneous neuronal population activity confined at a specific frequency

band. Thus, the connectivity strength could be measured by the probability that these regions co-activate during the nonstationary evolution of the frequency specific coupling. Applying this model on human ECoG data, we developed a novel approach for functional network parcellation. The accuracy and reproducibility of this approach were verified by clinical functional mapping methods (ECS and SSEP), and superior than the conventional method that only considers the long-term static correlation of the power envelope. Our analysis also revealed a dual-band scheme for the large-scale cortical connectivity and discovered that the carrier frequency ranging from alpha to beta (8–32 Hz) is for the resting state networking. The resting and different task states shared similar functional networks on the basis of this low carrier frequency. The probabilistic interaction and dual-band frequency coupling may provide a parsimonious neural mechanism in temporal and spectral domain to support intricate yet flexible network organization of human cortex, adding to the spatial organization principles found in fMRI studies (Glasser et al., 2016; Wang et al., 2019).

4.1. Nonstationary co-activation and microstates in resting state

With high temporal and spatial resolution, the ECoG signal has the capacity to capture the dynamic interaction of cortical regions in the resting state. Here, we quantified the band-limited co-activation of spontaneous neural population activities recorded by ECoG and found that the co-activation exhibited prominent fluctuations, in agreement with previous fMRI and EEG works (Allen et al., 2014; Calhoun et al., 2014; Shine et al., 2016; Wang et al., 2019). More importantly, our electrophysiological data supported the networking mechanism of the large-scale cortical regions as a probabilistic co-activation among a few microstates (Allen et al., 2014; Damaraju et al., 2014; Liu and Duyn, 2013). As shown in our ECoG data (Figs. 1 and 2), a certain cortical region could work with different regions in an interleaving fashion during the resting state, possibly corresponding to various basic working modes, as a basis of constructing various brain functions (Shine et al., 2016). We further postulated a dynamic networking mechanism: the more often two regions jointly participate in the same microstates, the stronger the interaction these two regions may have and the greater chance for them to form a functional network. This probabilistic co-activation has been reported by previous fMRI studies, which may require less metabolic energy while maintaining the brain in a

responsive state, compared with the scheme of static co-activation (Zalesky et al., 2014). For the first time, the current study provided electrophysiological evidence to support the findings in hemodynamic signals. Our observation, together with previous resting-state fMRI studies, can be seen as a network level substantiation of the Cell Assembly Theory, in which Hebb postulated that the growth of a neural assembly arose from the repeated co-activation of neural cells and populations (Hebb, 1949). The probabilistic co-activation observed here in our resting ECoG may act as the "transient, unstable reverberatory trace" between sensory stimuli "to induce lasting cellular changes that add to its stability" (Hebb, 1949). With the superior temporal resolution of ECoG, our next step is to further parse the detailed spatiotemporal structure of microstates that give rise to this "reverberatory trace", as that has been revealed partly in the resting fMRI at a low temporal resolution (Baker et al., 2014; Vidaurre et al., 2017).

4.2. Frequency multiplexing for cortical networking

In task states, most previous electrophysiological works have demonstrated the role of the high-gamma band (60–140 Hz) in synchronizing large-scale cortical activations (Cheung et al., 2016; Foster et al., 2015; Giraud and Poeppel, 2012; Qian et al., 2013; Si et al., 2017). Some of the studies also observed similar cross-region synchronization in the low-frequency band (6–16 Hz)(Buffalo et al., 2011). Recent studies started to reveal a more interesting scheme that implied that the brain adopts a multiplexing scheme to transmit information, with high frequency (high-gamma band) for bottom-up and low frequency (alpha and beta bands) for top-down stream (Bouton et al., 2018; Buschman and Miller, 2007; Fontolan et al., 2014; Rohenkohl et al., 2018). Here, in this study, our ECoG data suggested a similar dual-band multiplexing scheme for cortical connectivity in the human cortex: high carrier frequency for the task networks and a low carrier frequency for the resting network. This provided a frequency tagging and separation mechanism to bind different neuronal groups together into coordinated cell assemblies, while making it possible for different cortical networks to work together (Canolty et al., 2010; Harris, 2005).

Recent fMRI studies have revealed similar functional connectivity patterns between the resting and task-dependent states (Cole et al., 2014; Fox and Raichle, 2007), and the task performance can even be predicted individually by the resting fMRI (Cole et al.,

2016; Tavor et al., 2016). Our work provides electrophysiological evidence for the consistency of the large-scale functional connectivity among the resting and various states. We found similar spatial patterns of functional networks during the resting and various task states in the low carrier frequency range (Figs. 6 and 7D), while when taking the high gamma band as the carrier frequency, the functional connectivity patterns in the rest and different task states could be discriminated in a space with few principal components (Fig. 7C). Our finding suggested a new perspective of understanding the relationship between the resting and task networks: although they exist in the same cortical space and share similar spatial patterns, they may use a multiplexing scheme to maintain their connectivity over different carrier frequencies. The low- and high-frequency components contribute to the basic stability and task-specific differences, respectively (Laird et al., 2013). During task states, task-specific local activities were modulated to a high carrier-frequency, to code corresponding task-related information, while the large-scale connectivity between the arousing functional regions and other cortical regions keeps stable in the low carrier frequency to maintain the basic brain-wide functional architecture and facilitate the large-scale information process. The cross-frequency coupling (CFC) phenomenon found in various task states may act as a bridge between these two frequency systems (Canolty et al., 2010; Fontolan et al., 2014).

The carrier frequency ranging from alpha to beta was more accurate in parcellating cortical functional networks, which confirmed the dominant role of low frequency communication in large-scale networks as that has been found by previous MEG work (Hipp et al., 2012). In a detailed analysis, the optimal carrier frequencies for sensory and motor-related functional regions converged in the alpha to beta range. However, the hearing network in the temporal cortex and the frontal eye field exhibited slower carrier frequency for intra-network communication (Fig. 4B). This observation matched well with the intrinsic frequency of spontaneous cortical activities in respective functional networks (Frauscher et al., 2018)(Fig. 4A). Therefore, we deduced that the cortical interaction in the resting state may also happen in a multiplexing way encompassing neural oscillations in a broad low frequency range (Engel et al., 2013; Mantini et al., 2007; Nolte et al., 2008). The carrier frequency of the resting functional networks may be an intrinsic property of the "reverberatory trace" postulated by Hebb (Canolty et al., 2010; Hebb, 1949), which is very likely to be decided by the

intra-network connectivity pattern (Frauscher et al., 2018). On top of the low carrier frequency, we found that the spectral density of the band power envelope leaned toward the ultralow frequency range (<0.15 Hz, Fig. 4D), which is similar to the previous MEG finding (Hipp et al., 2012), and close to the main frequency range of the spontaneous BOLD signal (Fox et al., 2016; Fox and Raichle, 2007; Yeo et al., 2011). In addition, the connectivity patterns obtained from the electrophysiological signal resembled those from the fMRI. This implied that the spontaneous fluctuations of the BOLD signal may reflect the summation of ultra-slow power-envelope components over a broadband low-frequency range of underlying oscillation.

4.3. Clinical implication

Precise mapping of functional architecture of cortex is a crucial requirement in presurgical planning, especially for the neurosurgical patients with distorted functional networks, as in epilepsy and glioma. As the clinical 'gold standard', electrical cortical stimulation (ECS) is a precise but time-consuming procedure (Penfield and Roberts, 1959). Recently, both resting and task-based fMRI have shown great potential to improve the surgical planning procedures (Harrison et al., 2015). However, current fMRI still lacks enough accuracy and reproducibility for individual-level cortical mapping (Harrison et al., 2015). Our CAP approach allowed a resting ECoG-based parcellation of the individual functional networks with high inter-subject variability and test-retest reproducibility (Fig. 3). This task-free functional mapping demands a low time consumption (5–10 min) and could be utilized in patients that are incapable to execute specific tasks. Another difficulty of ECS is to map the brain networks relating to higher order functions, such as language, cognition and attention (Posner et al., 1988), which usually consist of distributed brain regions and are immune to local stimulations (Mesulam, 1990). In our CAP based parcellation, some separated regions with large distance were parcellated into the same functional networks in several patients and displayed similar spatial pattern with the language network (Fig. 3A, S1 and S5)(Hickok and Poeppel, 2007). These observations signified that our task-free ECoG based functional network parcellation may serve as pre-scoping for ECS to reduce search time of positive electrodes, as well as a reference for mapping the high-order functional networks.

4.4. Technical limitations

Although large area grid electrodes have been placed on the cerebral cortices in our experiments (electrode numbers ranging from 64 to 112), ECoG electrode arrays cannot provide complete cortical coverage, which remains a barrier for analyzing the large-scale functional connectivity across all cortical regions. In addition, ECS/SSEP tasks and electrode coverage are always concentrated in sensorimotor-related regions, which makes the parcellation validity in the association cortices still elusive and may possibly lead to deviations in the carrier frequency analysis.

In this study, we employed the monopolar reference which entailed a careful placement of the silent referencing electrodes (Leuthardt et al., 2004; Schalk et al., 2007; Si et al., 2017; Zhang et al., 2019). The common average reference (CAR) method has also been used in many ECoG studies (Chao et al., 2010; Cheung et al., 2016; Foster et al., 2015; Leonard et al., 2016). We re-ran the resting ECoG signals of two patients by employing the CAR method, and then calculated their co-activation probability (CAP) matrices as well as the parcellated cortical network patterns, following the same pipeline as we used in the previous analysis. The results are shown in Fig. S2. The similarity of the CAP matrices using monopolar and common-average references are r = 0.91 for patient S5 and r = 0.89 for patient S1, respectively. The functional parcellation after monopolar and common-average references are also similar. The dice-coefficient is 0.93 for patient S5 and 0.875 for patient S1 (Fig. S2). This result indicates that the CAP patterns are slightly influenced by the referencing methods. Although the optimal strategy of electrode referencing in intracranial EEG recording and analysis still requires further investigation (Li et al., 2018), in our study, since the CAP approach did not simply use the absolute values of functional connectivity (the electrodes in each microstate were spatially parcellated into sub-networks based on their averaged correlational patterns), it is immune to the global bias caused by the referencing method, thus may not change the electrode clustering and the final parcellation atlas.

Acknowledgements

This work was supported by the National Key R&D Program of China [grant number 2017YFA0205904 B.H.], National Science Foundation of China [grant number NSFC 61621136008], and the National Natural Science Foundation of China Grant

[grant number 61473169 B.H.]. The authors would like to thank Dan Zhang, Chen Song, Yue Ding, Yang Zhang, Rui Xu, Yili Yan, Li Shen, Xiaopeng Si, Ning Guo, Xiupeng Yan and Dongyang Li for their assistance and suggestions in the data processing and analysis; Hua Guo, Le He, and Yandong Zhu from Center for Biomedical Imaging Research of Tsinghua University for their assistance during MRI data collection.

From Quantum Bits to Frequency Vortices

Classical Orch OR term	FWT upgrade – what it really is
Tubulin π-electron cloud	**Resonant FM cavity** that traps standing acoustic-plasmon modes
Objective reduction	**Phase-lock collapse** when FM conservation in Φ hits instability threshold
Quantum bits (qubits)	**Frequency solitons** whose amplitude obeys $FM = ½ \rho \omega A^2$
Conscious moment	**Topologically closed FM loop** that persists ~40 ms before the next collapse

FWT replaces abstract qubits with concrete vibrational energy packets defined by:

$$FM = ½ \rho \omega A^2$$

$$L = ½(\partial_\mu \Phi)(\partial^\mu \Phi) - (\lambda/4)\Phi^4 - \kappa(\partial_\mu \Phi \partial_\nu \Phi)g^{\mu\nu}$$

These equations conserve energy-frequency product and allow macro-scale coherence without exotic gravity tweaks.